Why Amantadine Loses Its Function in Influenza M2 Mutants: MD Simulations

Chittima Laohpongspaisan,[†] Thanyada Rungrotmongkol,[†] Pathumwadee Intharathep,[‡] Maturos Malaisree,[†] Panita Decha,[†] Ornjira Aruksakunwong,[§] Pornthep Sompornpisut,[†] and Supot Hannongbua*,[†]

Department of Chemistry, Faculty of Science, Chulalongkorn University, Phayathai Road, Patumwan, Bangkok 10330, Thailand, and Department of Physics and Center of Nanoscience and Nanotechnology, Faculty of Science, Mahidol University, Rama 6 Road, Ratchathewi, Bangkok 10400, Thailand, and Department of Chemistry, Faculty of Science, Rangsit University, Pathumtani 12000, Thailand

Received August 4, 2008

Molecular dynamics simulations of the drug-resistant M2 mutants, A30T, S31N, and L26I, were carried out to investigate the inhibition of M2 activity using amantadine (AMT). The closed and open channel conformations were examined via non- and triply protonated H37. For the nonprotonated state, these mutants exhibited zero water density in the conducting region, and AMT was still bound to the channel pore. Thus, water transport is totally suppressed, similar to the wild-type channel. In contrast, the triply protonated states of the mutants exhibited a different water density and AMT position. A30T and L26I both have a greater water density compared to the wild-type M2, while for the A30T system, AMT is no longer inside the pore. Hydrogen bonding between AMT and H37 crucial for the bioactivity is entirely lost in the open conformation. The elimination of this important interaction of these mutations is responsible for the lost of AMT's function in influenza A M2. This is different for the S31N mutant in which AMT was observed to locate at the pore opening region and bond with V27 instead of S31.

1. INTRODUCTION

A highly pathogenic H5N1 variant avian influenza virus has resulted in symptomatic disease outbreaks throughout the world, causing large-scale deaths in poultry and the subsequent infection and death of over 200 humans since 2003.[1,2] An important and growing problem of resistance to available drugs, particularly when amantadine was used for influenza A virus outbreak control, has highlighted the need to understand the details at a molecular level of how drugs bind to and interact with their targets.

The M2 plays a vital role in the life cycle of the influenza A virus. The encoded protein consists of 97 amino acids and contains only a single transmembrane helix which is essential for M2 to function as part of a homotetrameric proton-selective channel.[3−5] Evidence from experimental studies suggests that the activation of the M2 channel involves protonation of H37.[3,5−12] Within neutral and basic *pH*, the M2 channel is closed, while proton permeation is observed following protonation of H37 at low *pH*. From NMR study, it has been proposed that it is the triply protonated H37 tetrad form that is likely to activate the channel.[13] This *pH* dependence study on ^{15}N chemical shift showed that in the absence of amantadine the bridge proton distributes its charge between imidazolium^{+}-imidazole nitrogens of the two H37. The detailed molecular mechanisms and structure basis of proton permeation in M2 channel requires very high-resolution structural techniques. A fine analysis of downfield shift of proton resonance[14] and vibrational spectroscopy study could give complementary information on hydrogen bonds of the studied system.[14,15] In addition, the N−H NMR relaxation experiments are powerful tools in elucidating insight into the molecular mechanism of protein function.[15] However, the well-known problems of protein size, expression, and stability under the studied conditions hamper ongoing efforts toward the understanding of the proton transport process. An additional complication associated with structural studies of membrane proteins is the fact that they are typically carried out in non-natural detergent micelles, which possibly alter their conformation to a variety of non-native states.[16−18]

Amantadine (1-adamantanamine hydrochloride) is a specific anti-influenza A drug that inhibits viral replication, primarily by binding to the M2 channel and thereby preventing proton conductance. Although amantadine is effective in the prophylaxis and treatment of all influenza A subtypes, it has been associated with central nervous system side effects. Moreover, an increasing and persistent resistance to adamantane in animals and humans has frequently been highlighted, especially in China and Hong Kong[19,20] which is of concern given that they are potentially some of the principal sources of new influenza variants. The adamantane-resistant levels have increased from below 10% during 1995−2002, rapidly growing to 58% in 2003, 74% in 2004, and 92% during 2005−2006.[20,16] The genetic analysis of emerging drug-resistance showed that the mutation is normally observed to take place at the residues within the transmembrane region, including the amino acids L26, V27, A30, S31, or G34.[21,22] The most commonly observed drug-resistance is caused by one of several single mutations, but

* Corresponding author phone: +66 22 187602; fax: +66 22 187603; e-mail: supot.h@chula.ac.th.
[†] Chulalongkorn University.
[‡] Mahidol University.
[§] Rangsit University.

10.1021/ci800267a CCC: $40.75
Published on Web 03/13/2009

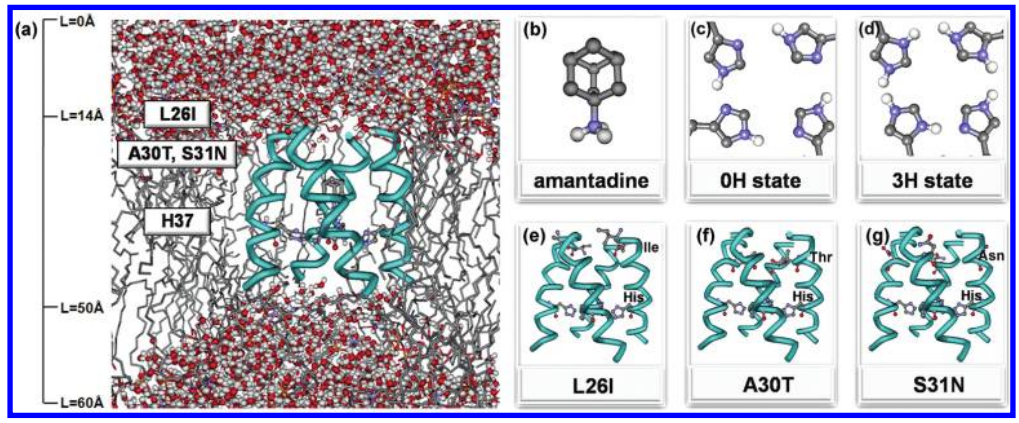

Figure 1. (a) Side view of the simulation system of the M2 channel with amantadine bound. L indicates the distance along a pore axis of the channel starting from the extracellular site. The average C^{α} positions of the start residue of the transmembrane helix is indicated by L = 14 Å. (b) Amantadine; (c) uncharged (0H) and (d) triple-protonated (3H) H37; (e) L26I, (f) A30T, and (g) S31N single mutant M2 strains.

variants with double substitution mutations have also been described.[19,21]

Recently, sequence analysis of the M2 gene of the influenza A H5N1 viruses from Vietnam, Malaysia, Cambodia, and Thailand showed that S31N and A30T are the most common mutations associated with resistance to amantadine.[23,24] Particularly, the A30T mutant exhibits extremely high-level resistance to amantadine with a 3300-fold compared to the IC_{50} value of the wild-type. Although the single-point mutation for L26I has not been found yet, the amantadine resistant single S31N and double L26I/S31N recombinant mutations have been reported with a 267-fold and unknown resistant level, respectively, compared to wild-type.

Based on experimental studies, two inhibitory mechanisms of action on the binding of drugs and wild-type M2 (WT-M2) were purposed: *i)* the drug blocks the channel by binding at the mouth of the pore,[11,25,26] and *ii)* the drug locates deeper in the channel and binds firmly to the side chains of H37.[27,28] These mechanisms were subsequently supported by both experimental and theoretical studies.[6,10,29,30] For these M2 mutants, however, an understanding of their altered interaction with amantadine is not yet known. Note that the emergence of drug-resistant influenza virus and the ever potential global pandemic risk has led to an urgent need to develop new highly potent drugs. This fact leads to the principle question of "Why does amantadine lose its function against the M2 mutants".

To address this question, molecular dynamics simulations (MD) of a series of three single M2 mutants (MT-M2), S31N, A30T, and L26I (see Figure 1e−g), complexed with amantadine were carried out in equilibrated lipid bilayer. The aim of this modeling was to try to elucidate and understand the effect of these M2 mutations on water transport in the presence of the amantadine. The simulations were focused on the closed[5,6,30] and open[6,10,30] states of the channel, represented by the channel with the neutral and triply protonated H37 tetrad, respectively.[5,10]

2. MATERIALS AND METHODS

2.1. Initial Structures of M2 Mutation Sequence and Their Complexes. The structural model of the WT-M2 obtained from solid state NMR experiments[13] was attained from the Protein Data Bank (entry code: 2H95) and used as the template structure for modeling the structures of the MT-M2. Three single mutants, L26I, A30T and S31N, were built from the WT-M2 structure using Discovery Studio 1.7 software.[31,32] The amantadine was then docked into the channel of MT-M2 proteins using the Autodock 3.0 program.[33]

2.2. Molecular Dynamics Simulations. For each mutant, we assigned all four H37 residues to be neutral for the simulations of the closed channel, whereas three out of the four H37 residues were positively charged for the open channel. The former is denoted hereafter as 0H (the non-protonated state) and the latter as 3H (the triple-protonated state) as shown in Figure 1c,d. Therefore, six systems were constructed for the simulations of the closed (0H) and open (3H) states of the three M2 mutants complexed with amantadine (AMT).

Each MT-M2 complex was inserted into pre-equilibrated lipid bilayer, containing 80 molecules of 1-palmitoyl-2-oleoyl-sn-glycerol-3-phosphatidylcholine (POPC) lipid[34] embedded in 2445 molecules of TIP3P water.[35] The systems were neutralized by the counter-ions, and the solvated box dimensions were set to 60 × 60 × 70 $Å^3$.

The simulations were carried out using the GROMACS 3.2.1 package[36] with GROMACS force field.[37] The Dundee PRODRG2[38] was used to generate the inhibitor's topology. In each case, the whole system was minimized with the steepest descent algorithm. Consequently, the systems were equilibrated for 0.5 ns with position restraints on the protein atoms, followed by 8 ns MD simulations. The structural coordinates from each simulation run were collected every 0.5 ps for analysis.

For all simulations, the periodic boundary condition with the NPT ensemble was employed. The LINCS algorithm[39] was applied to constrain bond lengths and angles involving hydrogen atoms, and a 2 fs time step was used. Systems were coupled separately to a Berendsen temperature bath[40] at 310 K, using a coupling constant τ_T of 0.1 ps. The constant pressure of 1 bar was kept constant by semi-isotropic coupling of the system to a Berendsen pressure bath.[40] Long-range interactions were involved within a twin-range cutoff: 1.2 nm for van der Waals interactions and 1.2 nm for electrostatic interactions computed using the Particle Mesh Ewald (PME) algorithm.[41] The analysis phase started from

4 to 8 ns in which the convergences of energies, temperature, pressure, and global root-mean-square displacement (rmsd) were used to verify the equilibrium of the systems. A side view of the simulation system of the M2 channel is shown in Figure 1a.

2.3. Free Energy Barrier for Water Permeation. The energy barrier of water transport throughout the M2 channel was calculated with an analogous treatment of reference.[42] The potential of mean force (pmf) of water along the channel axis can be derived from the density plot according to

$$\text{pmf} = -RT \ln w(r) \quad (1)$$

where R is the gas constant, T is temperature in Kelvin, and $w(r)$ is the probability density of water distribution in a spherical region within a radius of r. Here, the probability density is given as

$$w(r) = \rho_r/\rho_{\text{total}} \quad (2)$$

where ρ_r and ρ_{total} are the local and total water densities, respectively. In water density calculation, r is extended to 60 Å to ensure that water molecules in aqueous zone (bulk water) are taken into account. ρ_{total} represents the bulk waters which presumably have total probability equal or near to 1. By employing this assumption, ρ_{total} is the maximum value of ρ_r.

3. RESULTS AND DISCUSSION

To determine the effects of each single mutation on the function of M2 protein, water transport was monitored in terms of water density as a function of the distance (L) along a pore-axis of the channel starting from the extracellular site. In addition, distributions of amantadine (AMT) were analyzed to illustrate the movement of the drug and its location with respect to the histidine gate (H37) and a pore lining residue (A30). These results are summarized in Figure 2 and discussed below.

3.1. Water Density in the Channel. In the closed state (0H) of the WT-M2 channel (Figure 2a), zero water density was observed in the channel pore at 30 Å < L < 38 Å for the free and the AMT-bound forms at 27 Å < L < 33 Å. This suggested that water cannot penetrate through the channel with uncharged H37 in both the free and AMT-bound forms of the WT-M2 channel[29] and agrees well with previous theoretical studies.[6,30] With respect to the mutants, the AMT-bound mutants showed very similar water density plots to that of the wild-type, except for A30T. Thus, for both S31N and L26I zero water density was observed but with about 5 Å shifted distance compared to the WT-M2 (Figure 2b,d vs 2a). However, a slight degree of water density in the 0H state of AMT-bound A30T was detected (Figure 2c).

The water transport properties of the 3H state in both wild-type and mutant channels were significantly different from those of the 0H state. Apparently, all water density values in the 3H state were greater than zero.

Different water density between the WT-M2 and MT-M2 channels in the 3H state was also found. In the 3H state of the WT-M2 channel,[29] the minimum value of water density detected at L = 29 Å of the AMT-bound M2 was slightly smaller than that (L = 20 Å) of the free channel (Figure 2e). In the case of S31N, the water density plot shows its minimum value was comparable to that of the wild-type channel. However, a significantly different density profile was observed with a change in the minimum toward the A30 position (Figure 2f), with the increase in water density value at the minimum for A30T indicating that a greater amount of water can pass through the channel. Moreover, AMT appears to be no longer bound to the channel (Figure 2g), suggesting that AMT has lost its capability of blocking water transport in A30T. Based on the experimentally determined IC_{50} value of a previous study,[19] the A30T resistance mutation against AMT is some 3300-fold higher compared to the wild-type. Such mutation prevents the binding of the channel blocker and possibly facilitates the protein activity.

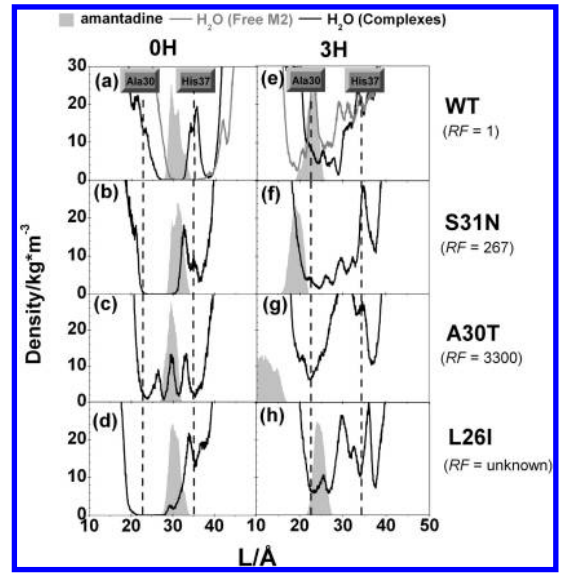

Figure 2. Water density (line) and AMT distribution (filled gray) along a pore axis of the WT and the three MT channels in the 0H and 3H states. The vertical dashed lines show the average C^{α} position of the four A30 and H37 residues. For comparison, the simulation data of the AMT-free (gray line) and AMT-bound (back line) WT-M2 shown in parts a−e are from a previous report.[29] *RF* stands for the resistant fold of AMT-resistance mutants compared to the WT-M2 strain.[19]

For L26I, water transport along the channel cannot take place in the 0H state, whereas water is more accessible through the pore in the 3H state than in both of the wild-type and S31N mutant M2. Thus, the L26I mutation could be expected to exhibit a higher resistance to AMT than the AMT-resistant S31N mutant, although this remains to be experimentally confirmed. However, the effect of the medium-level AMT-resistant mutant, S31N, remains unclear because the observed water densities do not significantly differ from those of the AMT blocked-WT complex.

Figure 3a−h shows the potential of mean force (pmf) derived from eq 1. The pmf profiles describe the free energy barrier for water transport along the channel. For the 0H state, the activation energy barriers are significantly high for the wild-type, S31N and L26I suggesting that water permeation is energetically unfavorable in these systems. However, mutation at A30 has caused a significant reduction of the free energy barrier for water transport. This is consistent with what was found in the water density plots (Figure 2a−d), where nonzero water density throughout the channel was detected only in the A30T (Figure 2c). In terms of peak position, an unfavorable energy barrier for wild-type (the

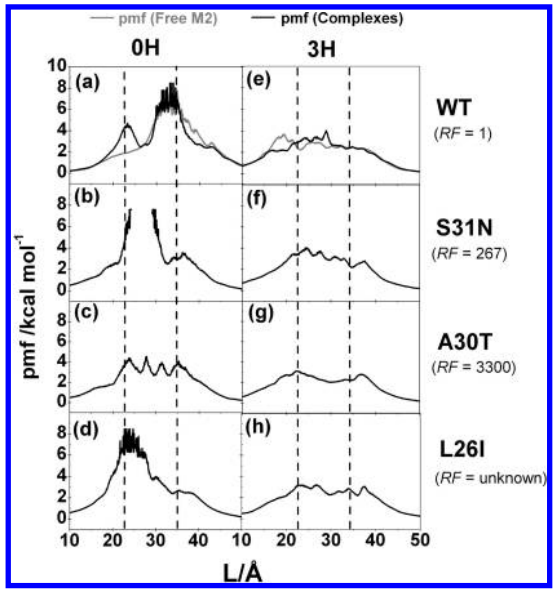

Figure 3. The potential of mean force (PMF) for water passage along the M2 pore. The figure legend appears on the graph is similar to Figure 2 except for the *y*-axis label.

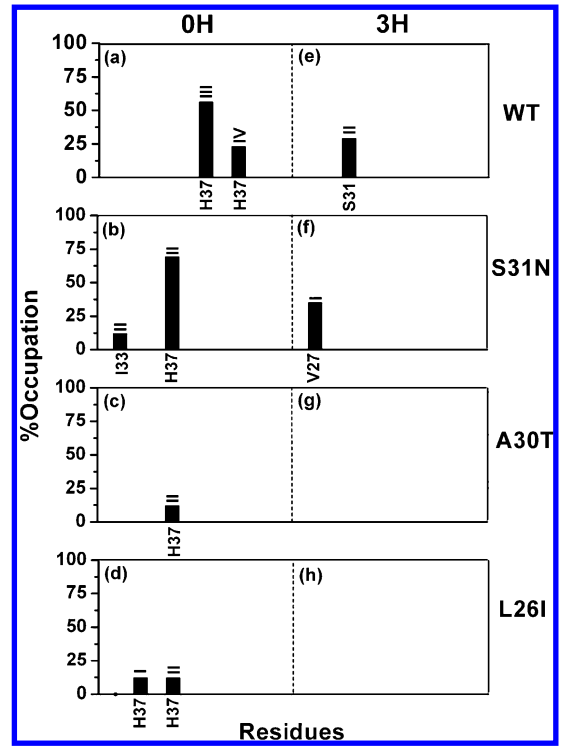

Figure 4. The percent occurrence as occupancy of the hydrogen bonding between M2 residues and AMT calculated from the WT-M2 and three MT-M2 proteins (S31N, A30T, and L26I) bound with AMT. Roman numerals above each bar refer to the M2 subunit monomer number (I, II, III, and IV, respectively).

higher peak in Figure 3a) was considerably shifted from the intracellular side (the right dashed line) toward the extracellular side of the pore (the left dashed line in Figure 3b−d) in the mutants.

Excluding the A30T, the calculated free energy barriers of the 3H state for both wild-type and mutants are significantly lower than those of the 0H state. This is in good agreement with the density plot shown in Figure 2 in which water density is higher in the 3H than 0H states.

3.2. AMT: Distribution and Interactions. A measure of AMT distribution in the M2 channel was already shown in Figure 2. In addition, the percentage occupancy of hydrogen bonds between AMT's ammonium group and the M2 protein was separately determined for the four subunits of the M2. The geometric criteria for hydrogen bonding were as follows: *(i)* a proton donor−acceptor distance of ≤3.5 Å and *(ii)* a donor-H-acceptor bond angle of ≥120°. The results are summarized in Figure 4.

In the case of AMT bound to either WT-M2 or the different MT-M2s in the 0H state, all AMT distributions (gray filled areas in Figure 2a−d) are likely to be located in the same position and approach considerably close to H37. These are mainly the results of both hydrogen bonding between the ammonium group of AMT and the immidazole ring of H37 and hydrophobic interactions between tricyclic adamantane and the tetrameric M2 channel pore. The percentage occupancy of hydrogen bonds in the two single L26I (both 12% for I and II; Figure 4d) and A30T mutants (12%; Figure 4c) were significantly lower than those of the wild-type strain (56 and 17% for III and IV, respectively; Figure 4a). For the S31N mutation, besides this conserved hydrogen bond with H37 (70% for II; Figure 4b), AMT additionally formed a hydrogen bond with I33 (12%). Note that the two peaks in Figure 4a,b,d represent the formation of only one hydrogen bond, consecutively, with two subunits of the M2 tetramer, and not two distinct hydrogen bonds.

In comparison to the AMT distribution in the 0H state, the distribution position of AMT in the 3H state was either shifted toward the extracellular end of the channel or was found to not be bound to the channel at all as is especially the case for the A30T mutant where AMT's position is completely outside the channel pore. This result is consistent with previous findings on the WT complex where AMT was located at the shallow region of the channel in the higher protonation states and subsequently interacted with the opening pore residues.[29] In terms of hydrogen bonds, the interaction was shifted from S31 in the wild-type to V27 in the S31N mutant with almost the same percentage occupancy (Figure 4e,f), while the AMT-target interactions of the two single A30T and L26I strains totally disappeared (Figure 4g,h). It seems most likely that loss of these hydrogen bonds in the A30T and L26I mutants of M2 is responsible for the transport of waters across the channel and thus gain of resistance to AMT. Moreover, the hydrogen bond data support two different binding sites, the opening pore residues[6,29,43,44] and the histidine gate.[13,29,43] Taking into account all this information the order of detected hydrogen bond occupations in the three mutations is S31N > L26I > A30T, and resistance to AMT is most likely caused by a decrease in the binding of AMT to the M2 residues, as noticeably revealed in the two single mutants, L26I and A30T.

In summary, the level of drug-resistant M2 strains can be explained by both the higher water-accessibility in the pore (section 3.1) and the lower affinity of AMT.

3.3. Solvation of AMT. To further explore the binding of AMT with surrounding waters, the number and percent occupation of hydrogen bonds were analyzed (Table 1). Apparently, only one hydrogen bond with an occurrence frequency of > 40% was the most preferable drug-solvation model of the wild-type M2 in both the 0H and 3H states. Interestingly, AMT that does not form hydrogen

Table 1. Percentage of Zero, Single, Double, and Triple H-Bonds (0-, 1-, 2-, and 3-Hb, Respectively) between AMT and Water in M2 Tetrameric Pores in the 0H and 3H States for S31N, A30T, and L26I Mutants and the Wild-Type

	% H-bond			
M2	0-Hb	1-Hb	2-Hb	3-Hb
0H State				
WT	23	43	16	18
S31N	1	18	77	4
A30T	2	18	47	33
L26I	1	10	39	50
3H State				
WT	25	42	26	7
S31N	1	13	52	34
A30T	1	15	38	46
L26I	1	13	59	27

bonds with water occupies 23 and 25% occurrence frequency in the 0H and 3H states, respectively. In contrast, AMT-bound M2 mutants of both states were mostly solvated via the formation of two or three hydrogen bonds. It should be noted that the number of hydrogen bonds between AMT and water molecules depends on the position of AMT in the M2 channel in which water can be accessible. In the case of the A30T mutant in the 3H state, triple hydrogen bonding AMT and water were found with the highest percentage occupancy (46%). The greater the number of hydrogen bonds between AMT and the solvent are, the weaker the interactions of AMT with the target M2 pore are. These solvation results suggested that interactions between AMT and the M2 mutants decrease significantly, particularly in the 3H state, and is a likely reason then why AMT loses its function in the M2 mutant strains. That is how these mutants gain resistance to AMT.

4. CONCLUSION

From our simulated results, the A30T and L26I mutations possibly affect amantadine (AMT) binding in the open state of the M2 channel and increase conducting water molecules. AMT distribution in the closed states is near the H37 residue of wild-type and mutants due to hydrogen bonding and hydrophobic interactions between the drug and the channel pore. The results of the open states of these mutants showed minimum water density values of > 0 as well as different AMT distributions. The A30T and L26I mutants substantially increase water transport with respect to the open state wild-type. The AMT remains near the extracellular mouth of all the wild-type and mutant M2 channels, except for A30T where AMT is completely unbound and hydrogen bonding of AMT with H37 disappears in the open state. Analysis of the drug solvation leads us to conclude that these mutations possibly preclude interactions between the AMT and the M2 pore residues and permit higher water accessibility to facilitate the water transport property.

ACKNOWLEDGMENT

The authors thank the Thailand Research Fund for financial support and the Commission on Higher Education for its Post-Doctoral program. This work was partially supported by the Center of Excellence for Petroleum, Petrochemicals, and Advanced Materials, Chulalongkorn University grant to P.S. The computing facilities were provided by the Computational Chemistry Unit Cell, Faculty of Science, Chulalongkorn University, the National Center for Genetic Engineering and Biotechnology, and the National Nanotechnology Center, Thailand.

REFERENCES AND NOTES

(1) Gambotto, A.; Barratt-Boyes, S. M.; de Jong, M. D.; Neumann, G.; Kawaoka, Y. Human infection with highly pathogenic H5N1 influenza virus. *Lancet* **2008**, *371*, 1464–1475.
(2) Yee, K. S.; Carpenter, T. E.; Cardona, C. J. Epidemiology of H5N1 avian influenza. *Comp. Immunol. Microbiol. Infect. Dis.* **2008**, . doi: 10.1016/j.cimid.2008.01.005.
(3) Wang, C.; Takeuchi, K.; Pinto, L. H.; Lamb, R. A. Ion channel activity of influenza A virus M2 protein: characterization of the amantadine block. *J. Virol.* **1993**, *67*, 5585–5594.
(4) Pinto, L. H.; Lamb, R. A. The M2 proton channels of influenza A and B viruses. *J. Biol. Chem.* **2006**, *281*, 8997–9000.
(5) Nishimura, K.; Kim, S.; Zhang, L.; Cross, T. A. The closed state of a H+ channel helical bundle combining precise orientational and distance restraints from solid state NMR. *Biochemistry* **2002**, *41*, 13170–13177.
(6) Chen, H.; Wu, Y.; Voth, G. A. Proton transport behavior through the influenza A M2 channel: insights from molecular Simulation. *Biophys. J.* **2007**, *93*, 3470–3479.
(7) Wang, C.; Lamb, R. A.; Pinto, L. H. Activation of the M2 ion channel of influenza virus: A role for the transmembrane domain histidine residue. *Biophys. J.* **1995**, *69*, 1363–1371.
(8) Venkataraman, P.; Lamb, R. A.; Pinto, L. H. Chemical rescue of histidine selectivity filter mutants of the M2 ion channel of influenza A virus. *J. Biol. Chem.* **2005**, *280*, 21463–21472.
(9) Okada, A.; Miura, T.; Takeuchi, H. Protonation of histidine and histidine-tryptophan interaction in the activation of the M2 ion channel from influenza A virus. *Biochemistry* **2001**, *40*, 6053–6060.
(10) Hu, J.; Fu, R.; Nishimura, K; Zhang, L.; Zhou, H. X.; Busath, D. D.; Vijayvergiya, V.; Cross, T. A. Histidines, heart of the hydrogen ion channel from influenza A virus: Toward an understanding of conductance and proton selectivity. *Proc. Natl. Acad. Sci.* **2006**, *103*, 6865–6870.
(11) Pinto, L. H.; Holsinger, L. J.; Lamb, R. A. Influenza virus M2 protein has ion channel activity. *Cell* **1992**, *69*, 517–528.
(12) Chizhmakov, I. V.; Geraghty, F. M.; Ogden, D. C.; Hayhurst, A.; Antoniou, M.; Hay, A. J. Selective proton permeability and *pH* regulation of the influenza virus M2 channel expressed in mouse erythroleukaemia cells. *J. Physiol.* **1996**, *494*, 329–336.
(13) Hu, J.; Fu, R.; Cross, T. A. The chemical and dynamical influence of the anti-viral drug amantadine on the M2 proton channel transmembrane domain. *Biophys. J.* **2007**, *93*, 276–283.
(14) Mildvan, A. S.; Massiah, M. A; Harris, T. K.; Marks, G. T.; Harrison, D. H. T.; Viragh, C.; Reddy, P. M.; Kovach, I. M. Short, strong hydrogen bonds on enzymes: NMR and mechanistic studies. *J. Mol. Struct.* **2002**, *615*, 163–175.
(15) Kern, D.; Zuiderweg, E. R. P. The role of dynamics in allosteric regulation. *Curr. Opin. Struct. Biol.* **2003**, *13*, 748–757.
(16) Klare, J. P.; Bordignon, E.; Doebber, M.; Fitter, J; Kriegsmann, J.; Chizhov, I; Steinhoff, H. J.; Engelhard, M. Effects of solubilization on the structure and function of the sensory rhodopsin II/transducer complex. *J. Mol. Biol.* **2006**, *356*, 1207–1221.
(17) Tate, C. G. Comparison of three structures of the multidrug transporter EmrE. *Curr. Opin. Struct. Biol.* **2006**, *16*, 457–464.
(18) Bezanilla, F. The voltage-sensor structure in a voltage-gated channel. *Trends Biochem. Sci.* **2005**, *30*, 166–168.
(19) Abed, Y.; Goyette, N.; Boivin, G. Generation and characterization of recombinant influenza A (H1N1) viruses harboring amantadine resistance mutations. *Antimicrob. Agents Chemother.* **2005**, *49*, 556–559.
(20) Barr, I. G.; Hurt, A. C.; Iannello, P.; Tomasov, C.; Deed, N.; Komadina, N. Increased adamantane resistance in influenza A (H3) viruses in Australia and neighbouring countries in 2005. *Antiviral Res.* **2007**, *73*, 112–117.
(21) Bright, R. A.; Medina, M. L.; Xu, X.; Perez-Oronoz, G.; Wallis, T. R.; Davis, X. M.; Povinelli, L.; Cox, N. J.; Klimov, A. I. Incidence of adamantane resistance among influenza A (H3N2) viruses isolated worldwide from 1994 to 2005: a cause for concern. *Lancet* **2005**, *366*, 1175–1181.
(22) Cheung, C. L.; Rayner, J. M.; Smith, G. J.; Wang, P.; Naipospos, T. S.; Zhang, J.; Yuen, K. Y.; Webster, R. G.; Peiris, J. S.; Guan, Y.; Chen, H. Distribution of amantadine-resistant H5N1 avian influenza variants in Asia. *J. Infect. Dis.* **2006**, *193*, 1626–1629.

(23) Hurt, A. C.; Selleck, P.; Komadina, N.; Shaw, R.; Brown, L.; Barr, I. G. Susceptibility of highly pathogenic A (H5N1) avian influenza viruses to the neuraminidase inhibitors and adamantanes. *Antiviral Res.* **2007**, *73*, 228–231.
(24) Ilyushina, N. A.; Govorkova, E. A.; Webster, R. G. Detection of amantadine-resistant variants among avian influenza viruses isolated in North America and Asia. *Virology* **2005**, *341*, 102–106.
(25) Astrahan, P.; Kass, I.; Cooper, M. A.; Arkin, I. T. A novel method of resistance for influenza against a channel-blocking antiviral drug. *Proteins* **2004**, *55*, 251–257.
(26) Hay, A. J. The action of adamantanamines against influenza A viruses: inhibition of the M2 ion channel protein. *Sem. Virol.* **1992**, *3*, 21–30.
(27) Zhong, Q.; Newns, D. M.; Pattnaik, P.; Lear, J. D.; Klein, M. L. Two possible conducting states of the influenza A virus M2 ion channel. *FEBS Lett.* **2000**, *473*, 195–198.
(28) Pinto, L. H.; Lamb, R. A. Controlling influenza virus replication by inhibiting its proton channel. *Mol. Biosyst.* **2007**, *3*, 18–23.
(29) Intharathep, P.; Laohpongspaisan, C.; Rungrotmongkol, T.; Loisruangsin, A.; Malaisree, M.; Decha, P.; Aruksakunwong, O.; Chuenpennit, K.; Kaiyawet, N.; Sompornpisut, P.; Pianwanit, S.; Hannongbua, S. How amantadine and rimantadine inhibit proton transport in the M2 protein channel. *J. Mol. Graphics Modell.* **2008**, *27*, 342–348.
(30) Kass, I.; Arkin, I. T. How pH opens a H+ channel: The gating mechanism of influenza a M2. *Structure* **2005**, *13*, 1789–1798.
(31) Marti-Renom, M. A.; Madhusudhan, M. S.; Sali, A. Alignment of protein sequences by their profiles. *Protein Sci.* **2004**, *13*, 1071–1087.
(32) Eswar, N.; Eramian, D.; Webb, B.; Shen, M.; Sali, A. Protein structure modeling with MODELLER. In *Current Protocols in Bioinformatics*; Baxevanis, A. D., Petsko, G. A., Stein, L. D., Stormo, G. D., Eds.; John Wiley & Sons, Inc.: New York, 2006; Vol. 15, pp 5.6.1−5.6.30.
(33) Morris, G. M.; Goodsell, D. S.; Halliday, R. S.; Huey, R.; Hart, W. E.; Belew, R. K.; Olson, A. J. Automated docking using a lamarckian genetic algorithm and and empirical binding free energy function. *J. Comput. Chem.* **1998**, *19*, 1639–1662.
(34) Tieleman, D. P.; Berendsen, H. J.; Sansom, M. S. An alamethicin channel in a lipid bilayer: molecular dynamics simulations. *Biophys. J.* **1999**, *76*, 1757–1769.
(35) Jorgensen, W.; Chandrasekhar, J.; Madura, J.; Impey, R.; Klein, M. Comparison of simple potential functions for simulating liquid water. *J. Chem. Phys.* **1983**, *79*, 926–935.
(36) Lindahl, E.; Hess, B.; van der Spoel, D. Gromacs 3.0: a package for molecular simulation and trajectory analysis. *J. Mol. Mod.* **2001**, *7*, 306–317.
(37) Hermans, J.; Berendsen, H. J. C.; van Gunsteren, W. F.; Postma, J. P. M. A consistent empirical potential for water-protein interactions. *Biopolymers* **1984**, *23*, 1513–1518.
(38) van Aalten, D. M.; Bywater, R.; Findlay, J. B.; Hendlich, M.; Hooft, R. W.; Vriend, G. PRODRG, a program for generating molecular topologies and unique molecular descriptors from coordinates of small molecules. *J. Comput.-Aided. Mol. Des.* **1996**, *10*, 255–262.
(39) Hess, B.; Bekker, H.; Berendsen, H. J. C.; Fraaije, J. G. E. M. LINCS: a linear constraint solver for molecular simulations. *J. Comput. Chem.* **1997**, *18*, 1463–1472.
(40) Berendsen, H. J. C.; Postma, J. P. M.; van Gunsteren, W. F.; DiNola, A.; Haak, J. R. Molecular dynamics with coupling to an external bath. *J. Chem. Phys.* **1984**, *81*, 3684–3690.
(41) Darden, T.; York, D.; Pedersen, L. Particle mesh Ewald: an N•log(N) method for Ewald sums in large systems. *J. Chem. Phys.* **1993**, *98*, 10089–10092.
(42) Raschke, T. M.; Levitt, M. Detailed hydration maps of benzene and cyclohexane reveal distinct water structures. *J. Phys. Chem. B* **2004**, *108*, 13492–13500.
(43) Duff, K. C.; Gilchrist, P. J.; Saxena, A. M.; Bradshaw, J. P. Neutron diffraction reveals the site of amantadine blockade in the influenza A M2 ion channel. *Virology* **1994**, *202*, 287–293.
(44) Gandhi, C. S.; Shuck, K.; Lear, J. D.; Dieckmann, G. R.; DeGrado, W. F.; Lamb, R. A.; Pinto, L. H. Cu (II) inhibition of the proton translocation machinery of the influenza A virus M2 protein. *J. Biol. Chem.* **1999**, *274*, 5474–5482.

CI800267A